International Journal of General Medicine

Dovepress
Taylor & Francis Group

Open Access Full Text Article

ORIGINAL RESEARCH

METTL16 Promotes Cerebral Ischemia-Reperfusion Injury via m^{6}A-Dependent Upregulation of TIPARP

Meiling Xiang, Jiemi Han, Zai Ye, Bimeng Chen, Hongbo Wang

Department of Neurology, Ningbo No.1 Hospital, Ningbo, Zhejiang, 315000, People's Republic of China

Correspondence: Hongbo Wang, Email cb2371@126.com

Background: Ischemic stroke leads to severe cerebral ischemia/reperfusion (I/R) injury, resulting in neuronal death and neurological deficits. The N^6-methyladenosine (m^{6}A) methyltransferase METTL16 has emerged as a key regulator of RNA metabolism, but its specific role and mechanism in ischemic stroke remain unclear.

Methods: A transient middle cerebral artery occlusion (MCAO) model was established in adult male C57BL/6J mice. METTL16 was knocked down via intracerebroventricular injection of shRNA-expressing lentivirus at 6 hours post-reperfusion. Cerebral infarct volume (TTC staining), neurological function (mNSS, adhesive removal, corner-turning, and rotarod tests), histopathology (H&E, TUNEL, Nissl, NeuN), and apoptosis-related protein expression were evaluated. Primary cortical neurons and astrocytes were subjected to oxygen-glucose deprivation (OGD). Cell apoptosis, LDH release, inflammatory cytokines (TNF-α, IL-1β), and synaptic protein (Synapsin-1, PSD-95) expression were assessed. The METTL16-TIPARP interaction and m^{6}A modification were analyzed by RIP and m^{6}A-RIP-qPCR. Protein stability was determined using cycloheximide chase assay. Rescue experiments were performed by overexpressing TIPARP in METTL16-depleted cells.

Results: METTL16 knockdown significantly reduced infarct volume, attenuated neuronal apoptosis and inflammation, and improved sensorimotor and coordination functions after MCAO. In vitro, METTL16 depletion protected neurons and astrocytes from OGD-induced apoptosis, cytokine release, and synaptic damage. Mechanistically, METTL16 directly bound to TIPARP mRNA and enhanced its m^{6}A modification, thereby stabilizing TIPARP transcripts and upregulating TIPARP protein expression. Critically, TIPARP overexpression completely abolished the protective effects of METTL16 knockdown against OGD-induced apoptosis and synaptic impairment.

Conclusion: METTL16 promotes cerebral I/R injury by stabilizing TIPARP mRNA via m^{6}A methylation, leading to elevated TIPARP expression. The METTL16-m^{6}A-TIPARP axis represents a novel pathogenic mechanism and a potential therapeutic target for ischemic stroke.

Keywords: stroke, neurons, astrocytes, METTL16, RNA methylation, TIPARP

Introduction

Ischemic stroke is a frequently occurring neurological disease and the leading cause of permanent disability worldwide.[1,2] It is accompanied by severe cerebral ischemia/reperfusion (I/R) injury, in which neurons undergo irreversible damage and cell death within hours of the initial insult.[3] In addition to the rapid loss of neurons in the ischemic core, delayed neuronal death also occurs in the surrounding penumbra, contributing to progressive neurological deficits.[4,5] Over the past decades, therapeutic advances for ischemic stroke have primarily centered on recanalization strategies, including intravenous thrombolysis with recombinant tissue-type plasminogen activator (rt-PA) and endovascular thrombectomy.[6,7] However, these interventions are severely limited by a narrow therapeutic time window—typically within 4.5 hours for rt-PA and up to 24 hours for selected patients undergoing thrombectomy—rendering the majority of stroke patients ineligible for such treatments.[8] Consequently, there is an urgent need to identify novel neuroprotective targets that act downstream of vascular occlusion.

Epigenetic regulatory mechanisms have garnered increasing attention in the pathophysiology of neurological disorders, including ischemic stroke.[9,10] Among these, N^6-methyladenosine (m^{6}A) has emerged as the most abundant internal mRNA modification in eukaryotes and a critical regulator of RNA metabolism, influencing splicing, stability, translation, and decay.[11,12] This dynamic modification is orchestrated by a tripartite system: "writers" (methyltransferases such as METTL3/METTL14 and METTL16), "erasers" (demethylases like FTO and ALKBH5), and "readers" (eg, YTHDF family proteins).[13]

https://doi.org/10.2147/IJGM.S561723
Received: 12 September 2025
Accepted: 14 March 2026
Published: 12 April 2026

While m^{6}A signaling has been implicated in both neuroprotection and neurodegeneration, its functional outcome is highly dependent on the specific writer enzyme and its target transcripts. For instance, METTL3-mediated m^{6}A modification can either exacerbate neuronal apoptosis by stabilizing pro-death mRNAs (eg, Bmf)[14] or promote recovery by enhancing axon regeneration,[15] illustrating its context-dependent duality.

Notably, METTL16—a less-studied but evolutionarily conserved m^{6}A methyltransferase—has distinct substrate specificity compared to the METTL3/14 complex. Unlike METTL3/14, which primarily modifies RRACH motifs in coding regions, METTL16 preferentially methylates structured RNAs, including U6 snRNA and the 3′ UTR of MAT2A mRNA, to regulate S-adenosylmethionine (SAM) homeostasis.[16,17] Emerging evidence suggests that METTL16 is expressed in the central nervous system and may play unique roles in neural gene regulation;[18] however, its function in ischemic brain injury remains unexplored. Given its capacity to directly modulate the stability of specific mRNAs under stress conditions,[18] we posited that METTL16 might contribute to post-ischemic gene dysregulation in a manner distinct from other m^{6}A writers.

Concurrently, TIPARP (TCDD-inducible poly[ADP-ribose] polymerase), a member of the PARP family, functions as a mono-ADP-ribosyltransferase and E3 ubiquitin ligase.[19] While its roles in cancer have been characterized—such as promoting the degradation of HIF-1α and c-Myc[20]—emerging data implicate TIPARP in neuroinflammation and neuronal injury. For example, TIPARP is upregulated in microglia upon inflammatory stimulation and modulates aryl hydrocarbon receptor (AhR)-dependent cytokine production.[21] Moreover, genetic deletion of Tiparp in mice attenuates neuronal loss in models of neurotoxicity, suggesting a potential detrimental role in certain neurological injury contexts.[22] Despite these clues, the regulation and explicit function of TIPARP in cerebral ischemia remain unknown.

Critically, although certain m^{6}A modifications have been associated with neuroprotective outcomes (eg, YTHDF1-mediated enhancement of synaptic protein translation after injury[23]), accumulating evidence indicates that specific m^{6}A "writers" can exert opposing, deleterious effects depending on their target transcripts. This context-dependent duality underscores the necessity of defining the precise roles of individual writers. We therefore hypothesized that the understudied writer METTL16 might drive pathogenic gene expression following ischemia. We focused on TIPARP as a compelling candidate downstream effector for two reasons: (1) it is a stress-responsive factor implicated in promoting neuronal death,[22] and (2) bioinformatic analysis of its mRNA sequence revealed potential structural motifs compatible with METTL16 binding and regulation (data not shown), a premise supported by METTL16's known preference for structured RNA substrates.[17]

In this study, we investigated the role of METTL16 in cerebral I/R injury and tested the hypothesis that it functions by epigenetically inducing TIPARP expression via m^{6}A methylation. We demonstrate that METTL16 exacerbates ischemic neuronal and astrocytic damage by installing m^{6}A modifications on Tiparp mRNA, thereby enhancing its stability and expression. Our findings reveal a previously unrecognized pathogenic epitranscriptomic axis in ischemic stroke and highlight METTL16 as a potential therapeutic target.

Materials and Methods

Ethical Approval and Animal Use

This study was conducted in strict accordance with the National Institutes of Health Guide for the Care and Use of Laboratory Animals (8th edition, 2011). All experimental protocols were approved by the Institutional Animal Care and Use Committee of Ningbo No.1 Hospital (Approval No. NB159792). Surgery was performed under sodium pentobarbital anesthesia (50 mg/kg, intraperitoneal injection), and all efforts were made to minimize animal suffering. At the experimental endpoint, mice were euthanized by cervical dislocation, consistent with the AVMA Guidelines for the Euthanasia of Animals (2020).

Animals and Grouping

Male C57BL/6J mice (20–22 g, 8–10 weeks old) were obtained from Beijing Vital River Laboratory Animal Technology Co., Ltd. (Beijing, China) and housed under standard specific pathogen-free (SPF) conditions (12-h light/dark cycle, 22 ± 1°C, 50–60% humidity) with ad libitum access to food and water. Mice were randomly assigned to sham or middle cerebral artery occlusion (MCAO) groups using a computer-generated random number table The investigators performing surgeries, behavioral tests, and histological analyses were blinded to group allocation throughout the study. Sample size was determined

a priori using G*Power 3.1 software based on pilot data and published studies ($\alpha = 0.05$, power = 0.8), resulting in n = 8–10 mice per group for in vivo experiments. Exact sample sizes for each assay are specified in the corresponding figure legends.

Animal Middle Cerebral Artery Occlusion (MCAO) Model

Transient focal cerebral ischemia was induced by intraluminal MCAO as previously described.[24] Briefly, mice were anesthetized with sodium pentobarbital and placed on a thermostatic heating pad to maintain core body temperature at 37.0 ± 0.5°C. A midline neck incision was made to expose the right common carotid artery (CCA), external carotid artery (ECA), and internal carotid artery (ICA). A silicone-coated nylon monofilament (diameter: 0.22 mm; Doccol Corporation, USA) was advanced from the ECA into the ICA to occlude the origin of the middle cerebral artery. After 60 minutes of occlusion, the filament was withdrawn to restore blood flow, and the incision was sutured. Sham-operated mice underwent identical procedures without filament insertion.

For intracerebroventricular (ICV) delivery, a lentiviral vector expressing short hairpin RNA targeting METTL16 (shMETTL16; target sequence: 5′-GCAUCUACUGAGAUUGAUATT-3′) or scrambled control shRNA (shCtrl) was used. Both constructs were designed and synthesized by GenePharma Co., Ltd. (Shanghai, China). Viral particles were resuspended in sterile nuclease-free PBS and injected (5 μL at 1 μL/min) unilaterally into the right lateral ventricle at 6 hours after reperfusion using a stereotaxic frame (RWD Life Science) with coordinates relative to bregma: anteroposterior (AP) −0.3 mm, mediolateral (ML) +1.0 mm, dorsoventral (DV) −2.5 mm. The needle was left in place for 5 minutes post-injection to prevent backflow. Knockdown efficiency of shMETTL16 was validated in preliminary in vivo experiments by quantitative PCR (qPCR), demonstrating a >70% reduction in METTL16 mRNA levels in the peri-infarct cortex at 24 h post-injection compared to shCtrl-treated mice (Supplementary Figure S1). Given that METTL16 functions primarily as an RNA-binding methyltransferase regulating RNA metabolism at the post-transcriptional level, robust mRNA knockdown is expected to significantly attenuate its biological activity.

Assessment of Neurological Functions

Neurological deficits were evaluated at 14 days post-surgery by investigators blinded to the experimental groups. To minimize learning effects and establish baseline performance, all mice underwent a 3-day preoperative training period prior to MCAO surgery. Four well-established behavioral tests were employed to comprehensively assess sensorimotor and cognitive impairments: (1) In the adhesive removal test, a small circular adhesive tape (~6 mm in diameter) was affixed to the plantar surface of each forepaw, and the time to contact and remove the tape was recorded, with a maximum trial duration of 120 seconds; (2) In the corner-turning test, mice were allowed to enter a 30° corner, and turning direction (left or right) was recorded over 10 consecutive trials; a laterality index was calculated as (right turns − left turns)/total turns to quantify sensorimotor asymmetry; (3) The modified neurological severity score (mNSS), a composite scale ranging from 0 (no deficit) to 18 (severe deficit), was used to evaluate integrated motor, sensory, reflex, and balance functions; (4) Motor coordination and endurance were assessed using the rotarod test, in which mice were placed on an accelerating rotarod (from 4 to 40 rpm over 5 minutes), and the latency to fall was recorded across three trials with a 15-minute inter-trial interval.

Triphenyl Tetrazolium Chloride (TTC) Staining

To quantify acute ischemic injury before the onset of significant tissue remodeling or edema resolution, infarct volume was assessed at 24 hours after MCAO. Mice were deeply anesthetized and transcardially perfused with ice-cold phosphate-buffered saline (PBS). Brains were rapidly removed and sectioned into 2-mm-thick coronal slices using a mouse brain matrix. Sections were incubated in 2% triphenyl tetrazolium chloride (TTC; Sigma-Aldrich, USA) at 37°C for 20 minutes in the dark. Viable tissue stained deep red due to mitochondrial dehydrogenase activity, whereas infarcted regions remained pale. Following staining, sections were fixed in 4% paraformaldehyde overnight, photographed under consistent lighting conditions, and analyzed using ImageJ software (NIH). To correct for edema-induced swelling in the ipsilateral hemisphere, infarct volume was calculated using the indirect method:

$$\text{Corrected infarct volume (\%)} = [\text{Contralateral hemisphere volume} - (\text{Ipsilateral non-infarcted volume})]/\text{Contralateral hemisphere volume} \times 100$$

A sample size of 8–10 mice per group was used for this analysis.

Histological Analysis

For chronic histopathological evaluation, brains were collected at 14 days post-MCAO. Tissues were fixed in 10% neutral buffered formalin for 48 hours, cryoprotected in 30% sucrose solution for an additional 48 hours, embedded in optimal cutting temperature (OCT) compound (Sakura Finetek), and serially sectioned into 20-μm-thick coronal slices using a cryostat (Leica CM1950). Multiple staining approaches were applied to assess neuronal integrity and cell death: Nissl staining with 0.1% cresyl violet (Sigma) was performed to evaluate neuronal morphology and survival in the peri-infarct cortex; immunofluorescence labeling was conducted by permeabilizing sections with 0.2% Triton X-100, blocking with 10% goat serum, and incubating overnight at 4°C with anti-NeuN primary antibody (1:500; Abcam, ab177487), followed by fluorophore-conjugated secondary antibodies (Invitrogen) for 1 hour at room temperature, with nuclei counterstained using DAPI; general tissue architecture was examined by hematoxylin and eosin (H&E) staining using a commercial kit (Beyotime, China); and apoptotic cells were detected via terminal deoxynucleotidyl transferase dUTP nick-end labeling (TUNEL) assay using an In Situ Cell Death Detection Kit (Roche, Germany) according to the manufacturer's instructions. TUNEL-positive cells were quantified in five randomly selected fields (×200 magnification) per section. A total of 6–8 animals per group were included in the histological analyses.

Primary Astrocytes and Neuron Culture

Primary cortical neurons were isolated from embryonic day 16–18 (E16–E18) C57BL/6J mouse embryos. Cortices were dissected, digested with 0.125% trypsin (Thermo Fisher Scientific) for 15 min at 37°C, triturated, and filtered through a 100-μm cell strainer. Cells were plated on poly-D-lysine-coated coverslips in Neurobasal medium supplemented with 2% B27 and 1% GlutaMAX (Gibco). Half of the medium was replaced every 3 days. Neuronal purity (>90%) was confirmed by immunostaining for MAP2 (Abcam).

Primary astrocytes were prepared from postnatal day 1–2 (P1–P2) mouse pups. Cortices were dissociated and cultured in DMEM/F12 with 10% FBS. After 10–14 days, microglia and oligodendrocyte precursors were removed by shaking at 200 rpm for 6 h at 37°C. Adherent astrocytes were used at passage 1. Astrocyte purity (>95%) was confirmed by GFAP immunostaining (Abcam).

Cell Transfection and Viral Transduction

For in vitro knockdown, neurons and astrocytes were transduced with lentiviral particles carrying shMETTL16 or shCtrl at an MOI of 20. For rescue experiments, METTL16-knockdown cells were subsequently transfected with a mouse Tiparp overexpression plasmid (pcDNA3.1-TIPARP; constructed by GenePharma Co., Ltd.) or an empty vector control using Lipofectamine 3000 reagent 24 hours prior to OGD exposure.

Oxygen-Glucose Deprivation (OGD) Model

The OGD duration of 6 hours was selected based on established protocols demonstrating reproducible sublethal injury in primary neural cultures without complete cell death.[25] Briefly, culture medium was replaced with glucose-free, serum-free DMEM, and cells were placed in an anaerobic chamber (Billups-Rothenberg) flushed with 95% N_2/5% CO_2 at 37°C for 6 h. Control cells were maintained in normal culture medium under normoxic conditions. Following OGD, cells were returned to complete medium and incubated under standard conditions for indicated recovery periods.

Western Blotting Assay

Cerebral tissues and neurons were homogenized in RIPA lysis buffer (Epizyme, China) to obtain total proteins. The protein content was measured by BCA kit. Then a total of 35 μg proteins were divided by SDS-PAGE gel and then blotted onto PVDF membranes. The blots were blocked in 5% non-fat milk in PBST, followed by reaction with specific primary antibodies target Bcl-2, Bax, caspase-3, Synapsin-1, PSD95, and β-actin overnight. Next day, blots were hatched in corresponding secondary antibodies for 1 hour. The blots were then probed by the ECL reagent (Millipore, USA).

Quantitative PCR (qPCR) Assay

Total RNA was extracted from peri-infarct cortical tissues or cultured cells using TRIzol reagent (Invitrogen). cDNA was synthesized using the PrimeScript RT Reagent Kit (Takara). qPCR was performed on a QuantStudio 5 system (Applied Biosystems) using SYBR Green Master Mix (Takara). Relative gene expression was calculated by the 2^−ΔΔCt method and normalized to β-actin. Primer sequences were:

METTL16:
Forward: 5′-AGGACCTGGATGAGGTGCTG-3′
Reverse: 5′-TGGTGGTAGATGCCGTAGCC-3′
TIPARP:
Forward: 5′-CAGCCCTACAGCAACAACCT-3′
Reverse: 5′-GTCCTTGGCATCTGGTTGTC-3′
β-actin:
Forward: 5′-CATCCGTAAAGACCTCTATGCCAAC-3′
Reverse: 5′-ATGGAGCCACCGATCCACA-3′
All primers exhibited amplification efficiencies of 90–110% ($R^2 > 0.99$).

Cell Apoptosis

Apoptosis was assessed using an Annexin V-FITC/PI Apoptosis Detection Kit (Yeasen Biotech, China) according to the manufacturer's instructions. Cells were analyzed by flow cytometry (BD FACSCanto II) within 1 hour of staining.

LDH Detection

Cytotoxicity was evaluated by measuring lactate dehydrogenase (LDH) release into the culture supernatant using a commercial kit (Beyotime, China). Absorbance was read at 490 nm using a microplate reader.

Enzyme Linked Immunosorbent Assay (ELISA)

Levels of pro-inflammatory cytokines (TNF-α, IL-1β, IL-6) in cell culture supernatants were quantified using ELISA kits (Abcam, MA, USA) following the manufacturer's protocols. Samples were assayed in duplicate.

RNA Immunoprecipitation (RIP) Experiment

RIP assays were performed using the EZ-Magna RIP Kit (Millipore) with anti-METTL16 antibody (Abcam, ab195372) or normal rabbit IgG as control. For m^6A-specific MeRIP, the Magna MeRIP m^6A Kit (Millipore) and anti-m^6A antibody were used. Immunoprecipitated RNA was purified and analyzed by qPCR for TIPARP enrichment, expressed as % input.

Statistics

Data are presented as mean ± standard deviation (SD). Normality of distribution was assessed using the Shapiro–Wilk test, and homogeneity of variances was evaluated using Levene's test. For comparisons between two groups, an unpaired two-tailed Student's *t*-test was used. For comparisons among multiple groups, one-way ANOVA (for single-factor comparisons) or two-way ANOVA (for comparisons involving two independent factors) was employed, followed by Tukey's or Sidak's post hoc test for multiple comparisons, as detailed in the respective figure legends. A P-value < 0.05 was considered statistically significant. All analyses were performed using GraphPad Prism 9.0.

Results

METTL16 Promotes Brain Injury After MCAO in vivo

To investigate the role of METTL16 in ischemic stroke, we subjected mice to middle cerebral artery occlusion (MCAO). Knockdown of METTL16 was achieved via intracerebroventricular injection of shRNA-expressing virus (validated in Supplementary Figure S1). At 14 days post-reperfusion, we assessed infarct volume and neurological function. TTC staining revealed that METTL16 knockdown significantly reduced the cerebral infarct size compared to the MCAO control group

(Figure 1A). Histological analysis further demonstrated that MCAO induced severe inflammatory cell infiltration (HE staining), increased neuronal apoptosis (TUNEL-positive cells), and a marked reduction in Nissl bodies and NeuN-positive neurons, all indicative of substantial neuronal damage. Notably, these pathological changes were markedly ameliorated by METTL16 depletion (Figure 1B). Neurological deficits were evaluated using a battery of behavioral tests. METTL16 knockdown significantly improved the modified neurological severity score (MNSS) (Figure 1C), shortened the time to contact and remove an adhesive patch in the adhesive removal test (Figure 1D and E), reduced the percentage of right turns in the corner-turning test (Figure 1F), and increased the latency to fall in the rotarod test (Figure 1G). These results collectively indicate that METTL16 deficiency alleviates sensorimotor and coordination impairments following cerebral ischemia. At the molecular level, MCAO led to decreased expression of the anti-apoptotic protein Bcl-2 and increased levels of the pro-apoptotic proteins Bax and cleaved caspase-3. METTL16 knockdown effectively reversed these alterations in apoptosis-related protein expression (Figure 1H and I). Together, these in vivo data demonstrate that METTL16 knockdown mitigates brain damage and functional deficits after ischemic stroke.

METTL16 knockdown alleviates OGD-induced injuries in neurons and astrocytes in vitroWe next examined the cellular effects of METTL16 using an oxygen-glucose deprivation (OGD) model on primary neurons and astrocytes. Flow cytometry analysis showed that OGD significantly increased the percentage of both early and late apoptotic cells, and this increase was substantially suppressed by METTL16 knockdown (Figure 2A). Consistently, the OGD-induced elevation in lactate dehydrogenase (LDH) release, a marker of cell death, was also reduced upon METTL16 depletion (Figure 2B). Western blot analysis confirmed that METTL16 knockdown upregulated Bcl-2 and downregulated Bax and cleaved caspase-3 in OGD-treated cells (Figure 2C). Furthermore, OGD stimulated the secretion of pro-inflammatory cytokines TNF-α and IL-1β, which was significantly inhibited by METTL16 knockdown (Figure 2D and E). Since synaptic integrity is crucial for neuronal function, we assessed the expression of synaptic proteins. OGD downregulated Synapsin-1 and PSD-95, indicating synaptic impairment, and METTL16 knockdown restored their expression levels (Figure 2F). These findings suggest that METTL16 depletion protects neurons and astrocytes from OGD-induced apoptosis, inflammation, and synaptic damage.

METTL16 Regulates TIPARP Expression via m^{6}A-dependent RNA Methylation

To elucidate the mechanistic link between METTL16 and ischemic injury, we explored its downstream target. RNA immunoprecipitation (RIP) assays revealed significant enrichment of both METTL16 and m^{6}A on TIPARP mRNA (Figure 3A and B), suggesting direct interaction and modification. Knockdown of METTL16 using two independent shRNAs (shMETTL16-1 and shMETTL16-2) significantly reduced the m^{6}A modification level on TIPARP mRNA (Figure 3C), concurrently decreasing both TIPARP mRNA and protein expression in neurons and astrocytes (Figure 3D and E). To assess the impact on RNA stability, we treated cells with the protein synthesis inhibitor cycloheximide (CHX, 100 μg/mL) and monitored TIPARP protein decay over time. In control cells, TIPARP protein degradation commenced approximately 6 hours after CHX treatment. In contrast, METTL16-depleted cells exhibited accelerated degradation, starting as early as 3 hours post-CHX treatment (Figure 3F), indicating that METTL16-mediated m^{6}A modification stabilizes TIPARP mRNA. Importantly, the expression of other established m^{6}A-regulated transcripts, such as MALAT1 and SOCS2, remained unchanged upon METTL16 knockdown (Supplementary Figure S2), underscoring the specificity of METTL16's regulation of TIPARP. These results establish that METTL16 promotes TIPARP expression through m^{6}A methylation-dependent enhancement of RNA stability.

The METTL16/TIPARP Axis Mediates Neuronal and Astrocytic Injury in vitro

To determine whether TIPARP functions downstream of METTL16 in regulating ischemic injury, we performed rescue experiments by overexpressing TIPARP in METTL16-depleted cells subjected to OGD. Flow cytometry analysis showed that OGD increased total apoptosis from 5.43% to 15.80% in neurons and from 5.24% to 16.39% in astrocytes. METTL16 knockdown reduced apoptosis to 10.27% and 10.40%, respectively. Critically, concomitant TIPARP overexpression completely abolished the protective effect of METTL16 knockdown, restoring apoptosis levels to 15.92% in neurons and 17.22% in astrocytes. Statistical analysis confirmed that apoptosis in the "OGD + shMETTL16 + TIPARP" group was significantly higher than in the "OGD + shMETTL16" group ($p < 0.001$ for both cell types) (Figure 4A). Accordingly, the beneficial effects of METTL16 knockdown on the expression of apoptosis-related proteins (Bcl-2, Bax,

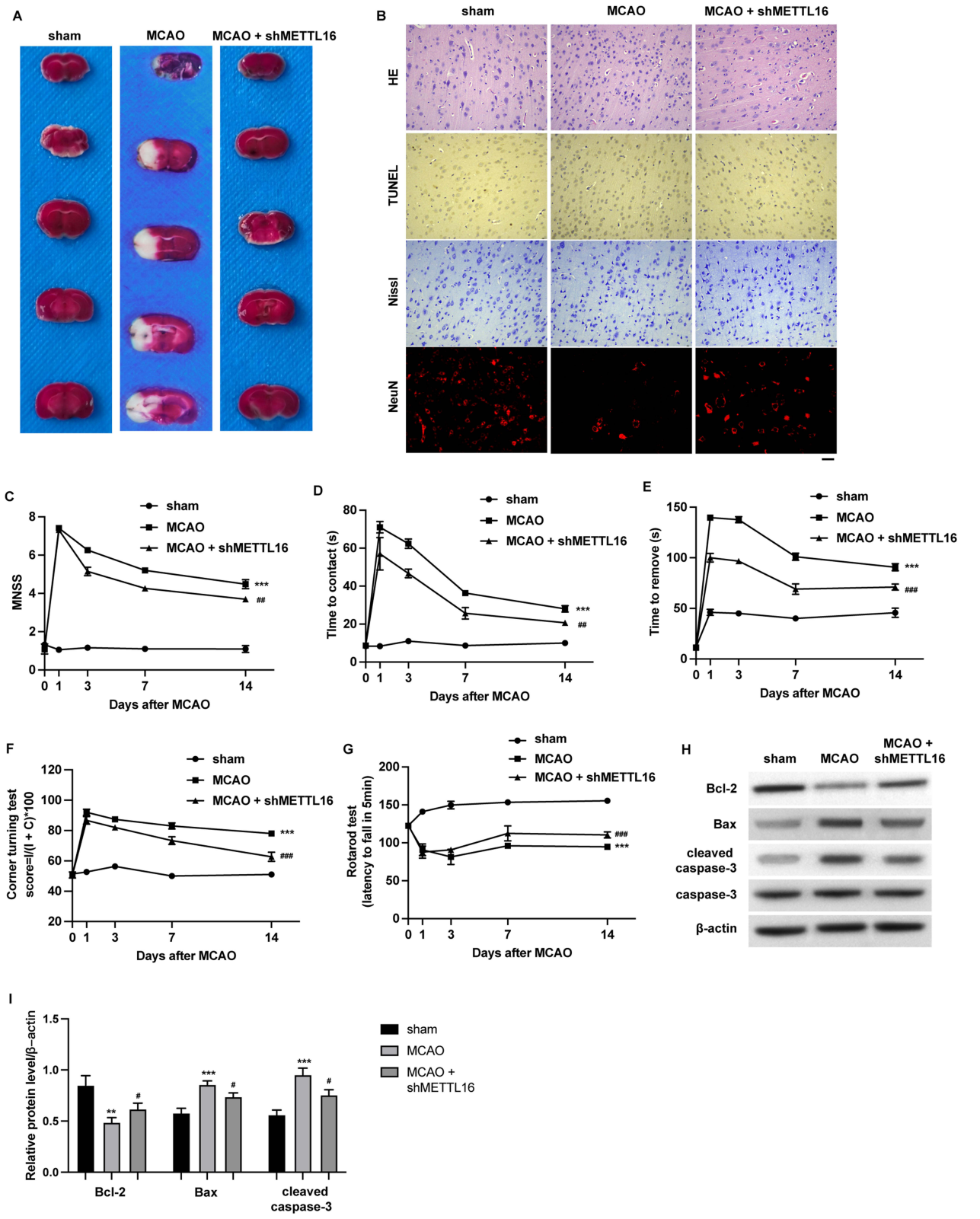

Figure 1 METTL16 promotes brain injury after MCAO in vivo. (**A**) Representative images of TTC-stained brain sections and quantification of infarct volume at 14 days after MCAO surgery. (**B**) Histopathological assessment of brain damage. HE staining shows inflammatory infiltration; TUNEL staining shows apoptotic cells (green); Nissl and NeuN staining show neuronal loss and damage. Scale bar, 50 μm. (**C**) Neurological deficits evaluated by the modified neurological severity score (MNSS). (**D** and **E**) Sensorimotor function assessed by the adhesive removal test, measuring time to contact (**D**) and time to remove (**E**) an adhesive patch. (**F**) Asymmetrical turning behavior assessed by the corner-turning test. (**G**) Motor coordination and balance evaluated by the latency to fall in the rotarod test. (**H** and **I**) Expression levels of apoptosis-related proteins (Bcl-2, Bax, cleaved caspase-3) in peri-infarct brain tissue analyzed by Western blot (**H**) and quantified (**I**). Data are presented as mean ± SD (n = 8–10 mice per group). $^{**}p < 0.01$, $^{***}p < 0.001$ vs. Sham; $^{\#}p < 0.05$, $^{\#\#}p < 0.01$, $^{\#\#\#}p < 0.001$ vs. MCAO + shNC (one-way ANOVA with Tukey's post hoc test).

https://doi.org/10.2147/IJGM.S561723

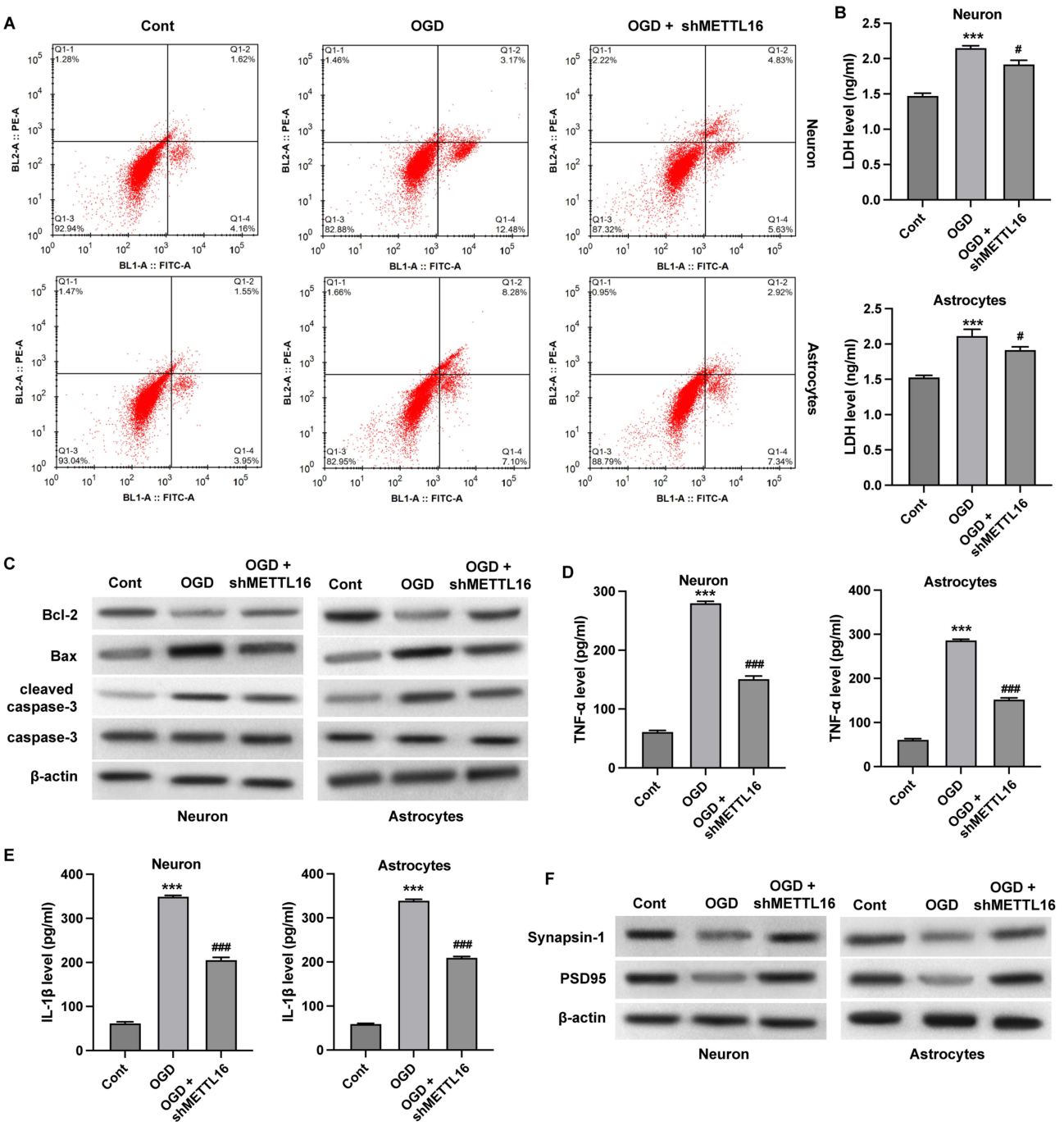

Figure 2 METTL16 knockdown alleviates OGD-induced injuries in neurons and astrocytes in vitro. Primary neurons and astrocytes were subjected to OGD with or without METTL16 knockdown. (**A**) Representative flow cytometry plots of cell apoptosis analyzed by Annexin V/PI staining (**B**) Cell death assessed by the release of lactate dehydrogenase (LDH). (**C**) Protein levels of apoptosis-related factors (Bcl-2, Bax, cleaved caspase-3) determined by Western blot. (**D** and **E**) Secretion of pro-inflammatory cytokines (**D**) TNF-α and (**E**) IL-1β measured by ELISA. (**F**) Protein expression of the synaptic markers Synapsin-1 and PSD-95 analyzed by Western blot. Data are mean ± SD from three independent experiments. ***p < 0.001 vs. Control; #p < 0.05, ###p < 0.001 vs. OGD + shNC (one-way ANOVA with Tukey's post hoc test).

cleaved caspase-3) (Figure 4B) and synaptic proteins (Synapsin-1, PSD-95) (Figure 4C) were also reversed by TIPARP overexpression. These data robustly demonstrate that TIPARP overexpression rescues the phenotype induced by METTL16 knockdown, confirming that TIPARP acts as a key downstream effector of METTL16 in promoting cellular injury during ischemic stress.

https://doi.org/10.2147/IJGM.S561723

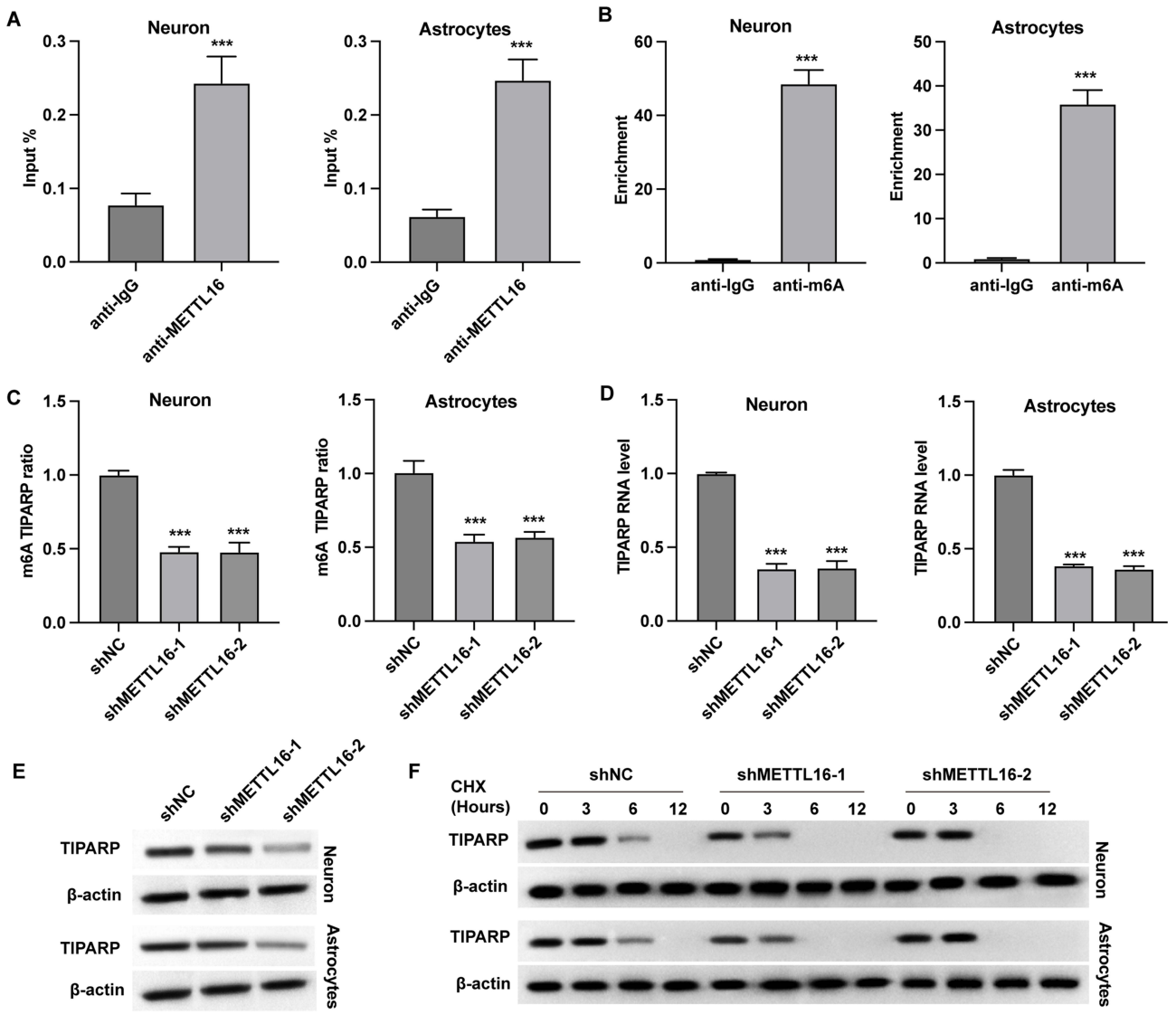

Figure 3 METTL16 regulates TIPARP expression via m^{6}A-dependent RNA methylation. (**A**) RNA immunoprecipitation (RIP) assay showing the binding of METTL16 to TIPARP mRNA in neurons and astrocytes. The abundance of TIPARP mRNA in the immunoprecipitates was quantified by qPCR and is presented as Input %. IgG was used as a negative control. (**B**) m^{6}A-RNA immunoprecipitation (MeRIP) assay showing the enrichment of m^{6}A modification on TIPARP mRNA in neurons and astrocytes, analyzed by qPCR. IgG was used as a negative control. (**C**) m^{6}A modification level on TIPARP mRNA measured by MeRIP-qPCR after METTL16 knockdown with two different shRNAs (shMETTL16-1 and shMETTL16-2). (**D** and **E**) Effects of METTL16 knockdown on (**D**) TIPARP mRNA levels (measured by qPCR) and (**E**) TIPARP protein expression (detected by Western blot). (**F**) Protein stability assay. Cells were treated with cycloheximide (CHX, 100 μg/mL) to inhibit new protein synthesis, and TIPARP protein levels were monitored by Western blot at the indicated time points (0, 3, 6, 12 h) after CHX addition. Quantification of band intensity relative to β-actin is shown below. Data are mean ± SD from three independent experiments. ***$p < 0.001$ vs. shNC or IgG (one-way ANOVA with Tukey's post hoc test).

Discussion

METTL16 contributes to cerebral ischemia-reperfusion injury and neurological deficits after ischemic stroke by promoting TIPARP expression via m^{6}A-dependent regulation.

This study identifies a previously unrecognized pathogenic axis in ischemic stroke, wherein the RNA methyltransferase METTL16 exacerbates cerebral ischemia-reperfusion injury by promoting the expression of TIPARP through m^{6}A-dependent post-transcriptional regulation.[26] Our findings, integrating in vivo neuroprotection and in vitro mechanistic dissection, position the METTL16/TIPARP axis as a crucial regulator of neuronal and glial fate following ischemic insult.

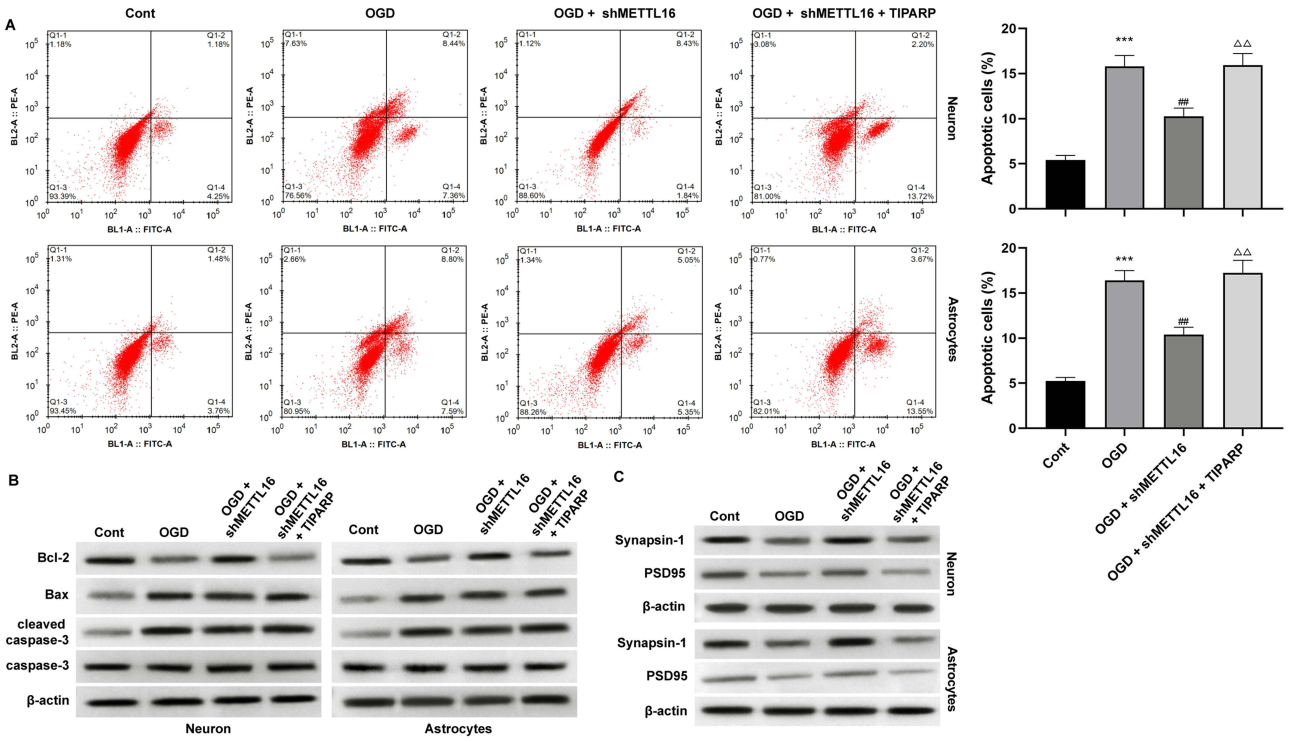

Figure 4 The METTL16/TIPARP axis mediates neuronal and astrocytic injury in vitro. Rescue experiments were performed by overexpressing TIPARP (OE-TIPARP) in METTL16-depleted neurons and astrocytes subjected to OGD. (**A**) Cell apoptosis was analyzed by flow cytometry. Representative flow plots (left) and quantification of total apoptosis (right) are shown. Statistical significance between the "OGD + shMETTL16" and "OGD + shMETTL16 + TIPARP" groups is indicated. (**B** and **C**) Protein expression analysis by Western blot for (**B**) apoptosis-related factors and (**C**) synaptic proteins. β-actin served as the loading control. Data are from three independent experiments (mean ± SD). ***p < 0.001 vs. Ctrl; ##p < 0.01 vs. OGD; ΔΔp < 0.01 vs. OGD + shMETTL16 (one-way ANOVA with Tukey's post hoc test).

METTL16 as a Detrimental Mediator in Ischemic Stroke

The role of m^{6}A modification in stroke is highly context- and writer-dependent, with reports describing both neuroprotective and detrimental outcomes.[26] Our data robustly demonstrate that METTL16 functions as a disease-aggravating factor. In vivo, METTL16 knockdown significantly reduced infarct volume and improved sensory, motor, and cognitive recovery after transient middle cerebral artery occlusion (MCAO) (Figure 1). This protective effect was associated with a reversal of apoptosis-related protein expression (Figure 1H–I). This aligns with emerging evidence implicating specific m^{6}A "writers" in stroke pathology. For instance, METTL3 has been shown to promote neuronal death by enhancing the stability of pro-apoptotic transcripts such as Bmf.[27] Our study extends this paradigm by identifying METTL16 as another key mediator, suggesting a coordinated yet distinct network of m^{6}A methyltransferases that fine-tune the post-ischemic transcriptome. Conversely, the reported neuroprotective role of m^{6}A via readers like YTHDF1 in supporting synaptic plasticity and memory after injury[28] highlights the functional complexity of the m^{6}A epitranscriptome. The divergent outcomes likely stem from the specificity of writer–target interactions and the differential recruitment of downstream reader proteins, underscoring the necessity of dissecting individual methyltransferases—as we have done here with METTL16.

Mechanistic Insight: METTL16 Regulates TIPARP via m^{6}A

A central finding of our study is the identification of TIPARP as a direct and specific functional target of METTL16 in ischemic neural cells. We provide multi-layered experimental validation: (1) METTL16 protein directly binds to Tiparp mRNA, as demonstrated by RNA immunoprecipitation (RIP) in both neurons and astrocytes (Figure 3A); (2) Tiparp transcripts are enriched for m^{6}A modifications, confirmed by m^{6}A-specific RIP (MeRIP) (Figure 3B); and (3) knockdown of METTL16 with two independent shRNAs markedly reduces both m^{6}A deposition on Tiparp mRNA (Figure 3C) and its steady-state mRNA and protein levels (Figure 3D and E). Furthermore, METTL16 depletion accelerated TIPARP protein degradation upon cyclohexamide treatment (Figure 3F), supporting that METTL16 promotes TIPARP expression through m^{6}A-mediated transcript

stabilization. Given that m^{6}A modifications are frequently recognized by reader proteins such as IGF2BP1–3, which enhance mRNA stability and translation,[29] the concurrent reduction in m^{6}A and Tiparp mRNA upon METTL16 depletion strongly suggests that METTL16 promotes TIPARP expression through m^{6}A-mediated transcript stabilization. Although direct measurement of Tiparp mRNA half-life was not performed in this study, the observed protein stability data align with this model, consistent with established principles of m^{6}A-dependent post-transcriptional regulation.[29,30] Importantly, the specificity of this regulatory axis is supported by the unchanged expression of other canonical m^{6}A targets—including MALAT1 and SOCS2—following METTL16 knockdown (Supplementary Figure S2). While METTL16's best-characterized role involves regulating MAT2A splicing to maintain S-adenosylmethionine (SAM) homeostasis,[31,32] our data reveal its capacity to directly modulate the abundance of specific protein-coding mRNAs like Tiparp under pathological stress, thereby expanding its functional repertoire beyond metabolic control.

Downstream Consequences: How TIPARP May Exacerbate Ischemic Injury

Functional rescue experiments definitively place TIPARP as the critical effector downstream of METTL16. Overexpression of TIPARP completely abolished the anti-apoptotic benefits conferred by METTL16 knockdown in oxygen-glucose deprivation (OGD)-treated neurons and astrocytes (Figure 4A), restoring apoptosis rates to levels comparable to OGD alone, and similarly reversed the effects on synaptic protein expression (Figure 4C). But how does elevated TIPARP drive cellular injury? TIPARP (TCDD-inducible poly(ADP-ribose) polymerase) is a mono-ADP-ribosyltransferase (mono-ART) and E3 ubiquitin ligase implicated in cellular stress responses.[33] We propose that its detrimental role in ischemia may involve multiple interconnected mechanisms.

First, although TIPARP exhibits weak PARP activity compared to PARP1, chronic upregulation could still contribute to NAD^+ depletion under energy-compromised conditions such as ischemia-reperfusion.[34] This aligns with the well-established neurotoxicity of PARP overactivation in stroke, where excessive ADP-ribosylation triggers AIF-mediated parthanatos.[35]

Second, as an E3 ubiquitin ligase, TIPARP may promote the degradation of pro-survival or anti-inflammatory proteins. For example, TIPARP has been shown to regulate the stability of aryl hydrocarbon receptor (AhR)-associated proteins, thereby modulating inflammatory gene expression in macrophages.[36] Given that AhR signaling is activated in microglia and astrocytes after stroke and contributes to neuroinflammation,[36] TIPARP-mediated modulation of this pathway could amplify cytokine production (eg, IL-1β, TNF-α)—consistent with our observation that METTL16 knockdown suppresses OGD-induced cytokine release (Figure 2D–E).

Third, recent work indicates that TIPARP can influence NF-κB transcriptional activity through ADP-ribosylation of key signaling intermediates,[37] a pathway centrally involved in post-ischemic inflammation.[9] Future studies should aim to identify the specific ubiquitination substrates and ADP-ribosylation targets of TIPARP in neurons and astrocytes under ischemic conditions, which could reveal novel nodal points for therapeutic intervention.

Limitations, Unanswered Questions, and Future Directions

Our study has several limitations that contextualize the findings and guide future research. First, we employed a global intracerebroventricular (ICV) knockdown approach, which does not distinguish the cell-autonomous contributions of METTL16 in neurons versus astrocytes. Given that both cell types express METTL16 and exhibit TIPARP-dependent injury, the relative importance of each compartment remains unclear. Second, while our in vitro rescue data using two cell types provide strong support for a linear METTL16–TIPARP axis, future in vivo rescue experiments would further solidify its pathological relevance in the intact organism. Third, the precise molecular link between TIPARP upregulation and the execution of apoptosis (eg, caspase-3 activation) or inflammation (eg, NLRP3 inflammasome assembly) requires deeper mechanistic exploration using genetic or pharmacological tools. Finally, the therapeutic window, delivery strategy, and potential off-target effects of METTL16 inhibition remain to be systematically evaluated.

Conclusion

In summary, we delineate a novel pathogenic circuit in ischemic stroke: Ischemic stress → upregulation/activation of METTL16 → increased m^{6}A modification of Tiparp mRNA → enhanced TIPARP expression → neuronal and astrocytic death via exacerbated metabolic stress and neuroinflammation (Graphical Abstract). This METTL16–m^{6}A–TIPARP axis

represents a new layer of post-transcriptional regulation in stroke pathology. From a translational perspective, our findings nominate METTL16 as a potential therapeutic target. Future work should focus on (1) developing selective METTL16 inhibitors or degraders; (2) generating neuron- and astrocyte-specific METTL16 knockout mice to dissect cell-type-specific contributions; and (3) mapping the TIPARP-dependent ubiquitinome and ADP-ribosylome in ischemic brain tissue to uncover druggable downstream effectors. These efforts will be essential to determine whether targeting this axis can safely improve outcomes after stroke.

Disclosure

The authors report no conflicts of interest in this work.

References

1. Saini V, Guada L, Yavagal DR. Global epidemiology of stroke and access to acute ischemic stroke interventions. *Neurology*. 2021;97(20 Suppl 2): S6–s16. doi:10.1212/wnl.0000000000012781
2. Quirke T, Sleator RD. A beginner's guide to genomics in complex neurological disorders. *Innov Discov*. 2024;1(4):29. doi:10.53964/id.2024029
3. Chen Y, Wu J, Yang Y, Xiong M, Yu X, Lei S. Causal effects of sarcopenia-related traits on ischemic stroke: a two-sample mendelian randomization study. *Clin Mol Epidemiol*. 2024;1:9. doi:10.53964/cme.2024009
4. Sharma D, Smith M. The intensive care management of acute ischaemic stroke. *Curr Opin Crit Care*. 2022;28(2):157–165. doi:10.1097/mcc.0000000000000912
5. Zhao Y, Zhang X, Chen X, Wei Y. Neuronal injuries in cerebral infarction and ischemic stroke: from mechanisms to treatment (Review). *Int J Mol Med*. 2022;49(2). doi:10.3892/ijmm.2021.5070
6. Hankey GJ. Stroke. *Lancet*. 2017;389(10069):641–654. doi:10.1016/s0140-6736(16)30962-x
7. Rikhtegar R, Yousefi M, Dolati S, et al. Stem cell-based cell therapy for neuroprotection in stroke: a review. *J Cell Biochem*. 2019;120 (6):8849–8862. doi:10.1002/jcb.28207
8. Phipps MS, Cronin CA. Management of acute ischemic stroke. *BMJ*. 2020;368:l6983. doi:10.1136/bmj.l6983
9. Zhang H, Shi X, Huang T, et al. Dynamic landscape and evolution of m6A methylation in human. *Nucleic Acids Res*. 2020;48(11):6251–6264. doi:10.1093/nar/gkaa347
10. Liu ZX, Li LM, Sun HL, Liu SM. Link between m6A modification and cancers. *Front Bioeng Biotechnol*. 2018;6(89). doi:10.3389/fbioe.2018.00089
11. Sun T, Wu R, Ming L. The role of m6A RNA methylation in cancer. *Biomed Pharmacother*. 2019;112(108613):108613. doi:10.1016/j.biopha.2019.108613
12. Tang Y, Chen K, Song B, et al. m6A-Atlas: a comprehensive knowledgebase for unraveling the N6-methyladenosine (m6A) epitranscriptome. *Nucleic Acids Res*. 2021;49(D1):D134–d43. doi:10.1093/nar/gkaa692
13. Oerum S, Meynier V, Catala M, Tisné C. A comprehensive review of m6A/m6Am RNA methyltransferase structures. *Nucleic Acids Res*. 2021;49 (13):7239–7255. doi:10.1093/nar/gkab378
14. Zhang B, Jiang H, Dong Z, Sun A, Ge J. The critical roles of m6A modification in metabolic abnormality and cardiovascular diseases. *Genes Dis*. 2021;8(6):746–758. doi:10.1016/j.gendis.2020.07.011
15. Su R, Dong L, Li Y, et al. METTL16 exerts an m(6)A-independent function to facilitate translation and tumorigenesis. *Nat Cell Biol*. 2022;24 (2):205–216. doi:10.1038/s41556-021-00835-2
16. Mermoud JE. The role of the m6A RNA methyltransferase METTL16 in gene expression and SAM homeostasis. *Genes*. 2022;13(12):2312. doi:10.3390/genes13122312
17. Satterwhite ER, Mansfield KD. RNA methyltransferase METTL16: targets and function. *Wiley Interdiscip Rev*. 2022;13(2):e1681. doi:10.1002/wrna.1681
18. Mansfield KD. RNA binding by the m6A methyltransferases METTL16 and METTL3. *Biology*. 2024;13(6):391. doi:10.3390/biology13060391
19. Gomez A, Bindesbøll C, Satheesh SV, et al. Characterization of TCDD-inducible poly-ADP-ribose polymerase (TIPARP/ARTD14) catalytic activity. *Biochem J*. 2018;475(23):3827–3846. doi:10.1042/bcj20180347
20. Ahmed S, Bott D, Gomez A, et al. Loss of the mono-ADP-ribosyltransferase, tiparp, increases sensitivity to dioxin-induced steatohepatitis and lethality. *J Biol Chem*. 2015;290(27):16824–16840. doi:10.1074/jbc.M115.660100
21. Bindesbøll C, Tan S, Bott D, et al. TCDD-inducible poly-ADP-ribose polymerase (TIPARP/PARP7) mono-ADP-ribosylates and co-activates liver X receptors. *Biochem J*. 2016;473(7):899–910. doi:10.1042/bj20151077
22. Zhang L, Cao J, Dong L, Lin H. TiPARP forms nuclear condensates to degrade HIF-1α and suppress tumorigenesis. *Proc Natl Acad Sci U S A*. 2020;117(24):13447–13456. doi:10.1073/pnas.1921815117
23. Wu F, Han B, Wu S, et al. Circular RNA TLK1 aggravates neuronal injury and neurological deficits after ischemic stroke via miR-335-3p/TIPARP. *J Neurosci*. 2019;39(37):7369–7393. doi:10.1523/jneurosci.0299-19.2019
24. Trotman-Lucas M, Gibson CL. A review of experimental models of focal cerebral ischemia focusing on the middle cerebral artery occlusion model. *F1000Research*. 2021;10:242. doi:10.12688/f1000research.51752.2
25. Ladak Z, Garcia E, Yoon J, et al. Sulforaphane (SFA) protects neuronal cells from oxygen & glucose deprivation (OGD). *PLoS One*. 2021;16(3): e0248777. doi:10.1371/journal.pone.0248777
26. Hong Y, Liu Q, Peng M, et al. High-frequency repetitive transcranial magnetic stimulation improves functional recovery by inhibiting neurotoxic polarization of astrocytes in ischemic rats. *J Neuroinflammation*. 2020;17(1):150. doi:10.1186/s12974-020-01747-y
27. Campbell BCV, De Silva DA, Macleod MR, et al. Ischaemic stroke. *Nat Rev Dis Primers*. 2019;5(1):70. doi:10.1038/s41572-019-0118-8
28. Toman NG, Grande AW, Low WC. Neural repair in stroke. *Cell Transplant*. 2019;28(9–10):1123–1126. doi:10.1177/0963689719863784

29. Liu Z, Chopp M. Astrocytes, therapeutic targets for neuroprotection and neurorestoration in ischemic stroke. *Prog Neurobiol*. 2016;144:103–120. doi:10.1016/j.pneurobio.2015.09.008
30. Song S, Huang H, Guan X, et al. Activation of endothelial Wnt/β-catenin signaling by protective astrocytes repairs BBB damage in ischemic stroke. *Prog Neurobiol*. 2021;199(101963):101963. doi:10.1016/j.pneurobio.2020.101963
31. Hayakawa K, Esposito E, Wang X, et al. Transfer of mitochondria from astrocytes to neurons after stroke. *Nature*. 2016;535(7613):551–555. doi:10.1038/nature18928
32. Chen M, Ma Q, Wariyapperuma Appuhamillage NMW, et al. Increased urinary albumin excretion but less damaged renal tubular structures in mice with genetically decreased elmo1 post ischemia/reperfusion injury. *Innov Discov*. 2026;3(1):4. doi:10.53964/id.2026004
33. Grimaldi G, Vagaska B, Ievglevskyi O, Kondratskaya E, Glover JC, Matthews J. Loss of tiparp results in aberrant layering of the cerebral cortex. *eNeuro*. 2019;6(6):ENEURO.0239–19.2019. doi:10.1523/eneuro.0239-19.2019
34. Hutin D, Long AS, Sugamori K, et al. 2, 3, 7, 8-Tetrachlorodibenzo-p-dioxin (TCDD)-inducible poly-ADP-ribose polymerase (TIPARP/PARP7) catalytic mutant mice (TiparpH532A) exhibit increased sensitivity to TCDD-induced hepatotoxicity and lethality. *Toxicol Sci*. 2021;183 (1):154–169. doi:10.1093/toxsci/kfab075
35. Huang P, Chen G, Jin W, Mao K, Wan H, He Y. Molecular mechanisms of parthanatos and its role in diverse diseases. *Int J Mol Sci*. 2022;23 (13):7292. doi:10.3390/ijms23137292
36. Rosado MM, Pioli C. ADP-ribosylation in evasion, promotion and exacerbation of immune responses. *Immunology*. 2021;164(1):15–30. doi:10.1111/imm.13332
37. Wang Y, Li Y, Ma C, et al. LncRNA XIST Promoted OGD-Induced Neuronal Injury Through Modulating/miR-455-3p/TIPARP Axis. *Neurochem Res*. 2021;46(6):1447–1456. doi:10.1007/s11064-021-03286-1
38. Han B, Zhang Y, Zhang Y, et al. Novel insight into circular RNA HECTD1 in astrocyte activation via autophagy by targeting MIR142-TIPARP: implications for cerebral ischemic stroke. *Autophagy*. 2018;14(7):1164–1184. doi:10.1080/15548627.2018.1458173